

This work was written as part of one of the author's official duties as an Employee of the United States Government and is therefore a work of the United States Government. In accordance with 17 U.S.C. 105, no copyright protection is available for such works under U.S. Law.

Public Domain Mark 1.0

<https://creativecommons.org/publicdomain/mark/1.0/>

Access to this work was provided by the University of Maryland, Baltimore County (UMBC) ScholarWorks@UMBC digital repository on the Maryland Shared Open Access (MD-SOAR) platform.

Please provide feedback

Please support the ScholarWorks@UMBC repository by emailing scholarworks-group@umbc.edu and telling us what having access to this work means to you and why it's important to you. Thank you.

PROCEEDINGS OF SPIE

SPIDigitalLibrary.org/conference-proceedings-of-spie

Plasmon-enhanced optical trapping of individual metal nanorods

Matthew Pelton, Mingzhao Liu, Kimani Toussaint, Hee Kim, Glenna Smith, et al.

Matthew Pelton, Mingzhao Liu, Kimani C. Toussaint Jr., Hee Y. Kim, Glenna Smith, Jelena Pesic, Philippe Guyot-Sionnest, Norbert F. Scherer, "Plasmon-enhanced optical trapping of individual metal nanorods," Proc. SPIE 6644, Optical Trapping and Optical Micromanipulation IV, 66441C (5 September 2007); doi: 10.1117/12.741857

SPIE.

Event: NanoScience + Engineering, 2007, San Diego, California, United States

Plasmon-enhanced optical trapping of individual metal nanorods

Matthew Pelton^{*,a}, Mingzhao Liu^b, Kimani C. Toussaint, Jr.^d, Hee Y. Kim^b, Glenna Smith^b, Jelena Pesic^b, Philippe Guyot-Sionnest^{b,c,d}, and Norbert F. Scherer^{a,c,d}

^aCenter for Nanoscale Materials, Argonne National Laboratory,
9700 S. Cass Ave., Argonne, IL 60439

^bDept. of Chemistry, ^cDept. of Physics, and ^dJames Franck Institute, University of Chicago,
929 E 57th Street, Chicago, IL 60637

ABSTRACT

We demonstrate three-dimensional optical trapping and orientation of individual Au nanorods, Au/Ag core/shell nanorods, and Au bipyramids in solution, using the longitudinal surface-plasmon resonance to enhance optical forces. Laser light that is detuned slightly to the long-wavelength side of the resonance traps individual and multiple particles for up to 20 minutes; by contrast, light detuned to the short-wavelength side repels rods from the laser focus. Under stable-trapping conditions, the trapping time of individual particles depends exponentially on laser power, in agreement with a Kramers escape process. Trapped particles have their long axes aligned with the trapping-laser polarization, as evidenced by a suppression of rotational diffusion about the short axis. When multiple particles are trapped simultaneously, evidence of interparticle interactions is observed, including a nonlinearly increasing two-photon fluorescence intensity, increasing fluorescence fluctuations, and changing fluorescence profiles as the trapped particle number increases.

Keywords: Optical trapping, plasmons, nanoparticles

1. INTRODUCTION

The use of optical forces to trap and manipulate micron-scale particles in solution is a well-established technique with widespread applications, including the controlled assembly of particles into arbitrary configurations; the precise application of forces to biological structures, from single cells down to single molecules; sensitive particle fractionation; and measurement of many-body colloidal interactions.¹ All these applications would benefit from the extension of optical trapping to nanometer-scale particles. However, the optical gradient force responsible for trapping is proportional to the particle volume in the Rayleigh regime, so that the trapping force on nanoparticles is generally weak and easily overwhelmed by thermal fluctuations and by radiation pressure. Only a limited number of experiments have demonstrated stable, three-dimensional trapping of objects with nanometer-scale dimensions. Objects such as carbon nanotubes² and semiconductor nanowires,³ for example, can be trapped because of their micron-scale extension in one dimension. As well, gold spheres with diameters down to 20 nm can be trapped by taking advantage of their large refractive index in the infrared,⁴ but achieving stable, three-dimensional trapping is difficult,⁵ and is accompanied by significant heating.⁶

It is possible to overcome many of these difficulties, enhancing trapping forces while avoiding unacceptable levels of heating, by taking advantage of optical resonances. As early as 1977, it was observed that Mie resonances enhance the

* pelton@anl.gov; phone 1-630-252-4598

The submitted manuscript has been created by UChicago Argonne, LLC, Operator of Argonne National Laboratory ("Argonne"). Argonne, a U.S. Department of Energy Office of Science laboratory, is operated under Contract No. DE-AC02-06CH11357. The U.S. Government retains for itself, and others acting on its behalf, a paid-up nonexclusive, irrevocable worldwide license in said article to reproduce, prepare derivative works, distribute copies to the public, and perform publicly and display publicly, by or on behalf of the Government.

radiation pressure on optically levitated dielectric spheres,⁷ and the first experimental report of laser tweezers includes a proposal for resonant enhancement of trapping forces.⁸ Shortly afterwards, resonant optical trapping of neutral atoms was demonstrated,⁹ and this now serves as the basis of a highly developed technology. Theoretical work has developed the idea of resonance enhancement for the room-temperature trapping of particles in solution,¹⁰ but experimental success has been limited. Resonances have been shown to slow down the diffusion of single molecules in solution,¹¹ and it has been proposed that excitonic transitions in semiconductor nanocrystals could permit their optical trapping,¹² but the trapping forces in these cases are limited by the broad linewidths and low saturation intensities of the transitions. Room-temperature trapping times are therefore limited to a few milliseconds, and stable trapping would require operation at liquid-helium temperatures.¹³

Nanoparticles of noble metals such as silver and gold, on the other hand, exhibit very strong plasmon resonances, associated with the collective oscillation of conduction electrons in the particle, and these resonances have very high saturation intensities.¹⁴ Metal nanorods, in particular, exhibit a strong longitudinal-plasmon resonance, corresponding to electron oscillation along the long axis of the rods, whose frequency can be tuned throughout the visible and near-infrared frequency range by controlling the aspect ratio and composition of the rods.¹⁵ The optical gradient force is enhanced if the trapping laser is tuned to the long-wavelength side of this resonance, with a maximum when the detuning is equal to half the resonance linewidth. Furthermore, since the longitudinal plasmon is excited only by light that is parallel to the long axis of the rod, the induced dipole will depend on the angle between the long axis of the rod and the trapping-laser polarization. A trapped particle will experience a torque if its long axis is out of alignment with the laser polarization, and will be brought back into alignment.

We have demonstrated this plasmon-resonance-enhancement based optical trapping technique to trap and orient a variety of individual metal nanoparticles in solution, including Au nanorods,¹⁶ Au/Ag core/shell nanorods, and Au bipyramids.¹⁷ Two-photon fluorescence is used to monitor the position of the nanorods in the trap, revealing that individual nanorods can be trapped for over 20 minutes. Multiple particles can be loaded into the trap, one at a time, and held for several minutes; in this case, the amplitude and noise in the fluorescence signal increase nonlinearly with the particle number, indicating an optical interaction amongst the trapped particles.¹⁷

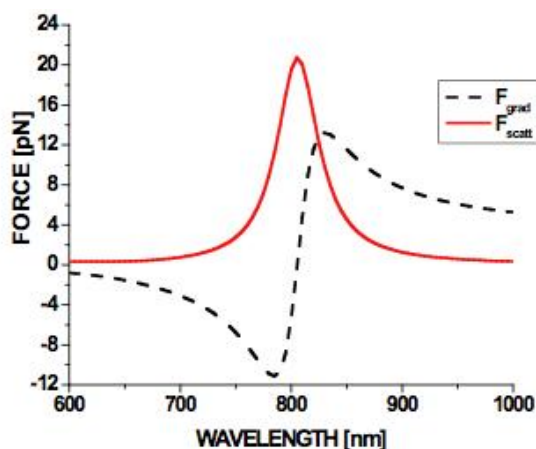


Fig. 1. Simulated optical gradient force (solid curve) and scattering force (dashed curve) acting on an Au ellipsoid with a short axis of 15 nm and long axis of 60 nm. The model is valid in the Rayleigh limit and assumes that the polarization of the optical field is parallel to the long axis of the rod.

2. THEORY

The ability of plasmon resonances to enhance optical trapping forces has been verified through detailed calculations,¹⁸ but the principle can be illustrated using a simple model. We model an Au nanorod as a prolate ellipsoid, and apply the quasi-static approximation, valid for particles that are small compared to the optical wavelength.¹⁵ When the incident light is polarized along the long axis of the rod, the polarizability of the particle is given by

$$\alpha = V \frac{\varepsilon - \varepsilon_m}{\varepsilon_m + L(\varepsilon - \varepsilon_m)} \quad , \quad (1)$$

where V is the volume of the rod, ε is the dielectric function of gold, ε_m is the dielectric constant of the surrounding medium (water, for our experiments), and L is the following geometrical factor:

$$L = \frac{1 - e^2}{e^2} \left(\frac{1}{2e} \ln \frac{1 + e}{1 - e} - 1 \right), \quad (2)$$

where e is the eccentricity of the ellipsoid.

Figure 1 shows calculated gradient and radiation-pressure forces acting on an Au nanorod, assuming a 100 mW beam focused to a diffraction-limited spot, and using tabulated values for the dielectric function of gold.¹⁹ The gradient force is significantly increased when the trap laser wavelength is detuned to the long-wavelength side of the longitudinal plasmon resonance. An optimal detuning for Au nanorods is approximately 50 nm, where the trap potential depth is several times greater than thermal energy at room temperature.

3. EXPERIMENTAL

3.1 Nanoparticle synthesis

The nanoparticles studied are chemically synthesized using a seed-mediated growth process, based on modifications of an established process for the growth of Au nanorods.²⁰ The growth of all particles starts with the preparation of very small gold-nanoparticle seeds, prepared by reducing HAuCl_4 with NaBH_4 . In order to produce Au nanorods, it is necessary to start with single-crystal seeds. These are produced by first mixing 0.25 mL of 10 mM HAuCl_4 with 10 mL of a 0.1 M CTAB solution at 30 °C. Next, 0.60 mL of a freshly prepared 10 mM NaBH_4 solution is injected quickly into the solution under vigorous stirring. The gold sol is stirred for at least 5 min, to allow for the complete decomposition of excess NaBH_4 .

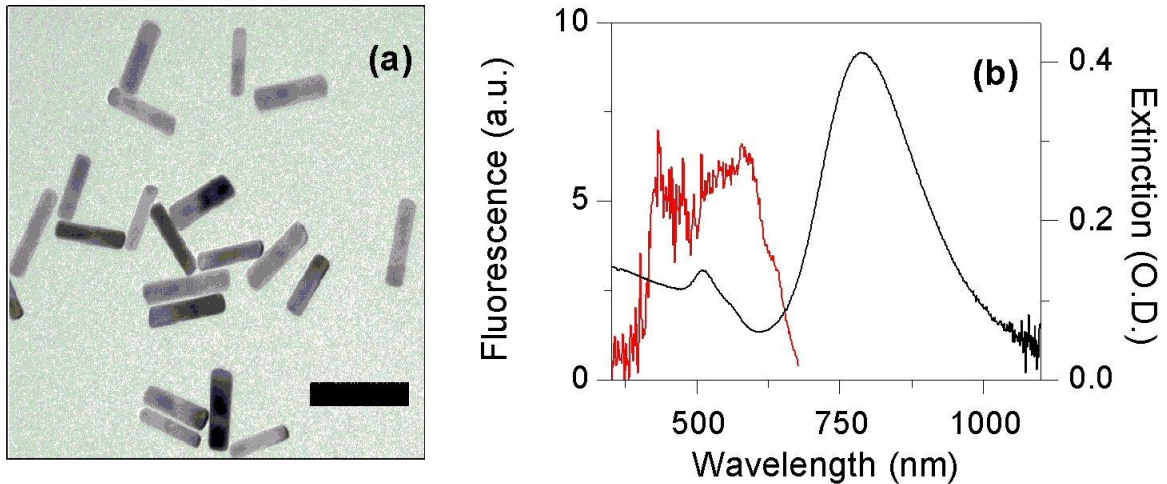


Fig. 2. (a) Transmission-electron-microscope image of Au nanorods. The scale bar is 50 nm. (b) Measured extinction spectrum of the Au-nanorod ensemble (right), and collected two-photon fluorescence spectrum (left). The fluorescence is cut off at longer wavelengths by optical filters.

Once the seeds are prepared, the nanorods are grown. 0.5 mL of 10 mM HAuCl_4 and 0.1 mL of 10 mM AgNO_3 are mixed with 10 mL of a 0.1 M CTAB solution. The solution is then acidified with 0.2 mL of 1.0 M HCl , followed by the addition of 0.08 mL of 0.1 M L-ascorbic acid, which reduces Au(III) to Au(I) . Finally, 24 μL of gold seeds are injected into the growth solution. The growth reaction is performed at 30 $^\circ\text{C}$ under gentle stirring, and ends within 2 hr.

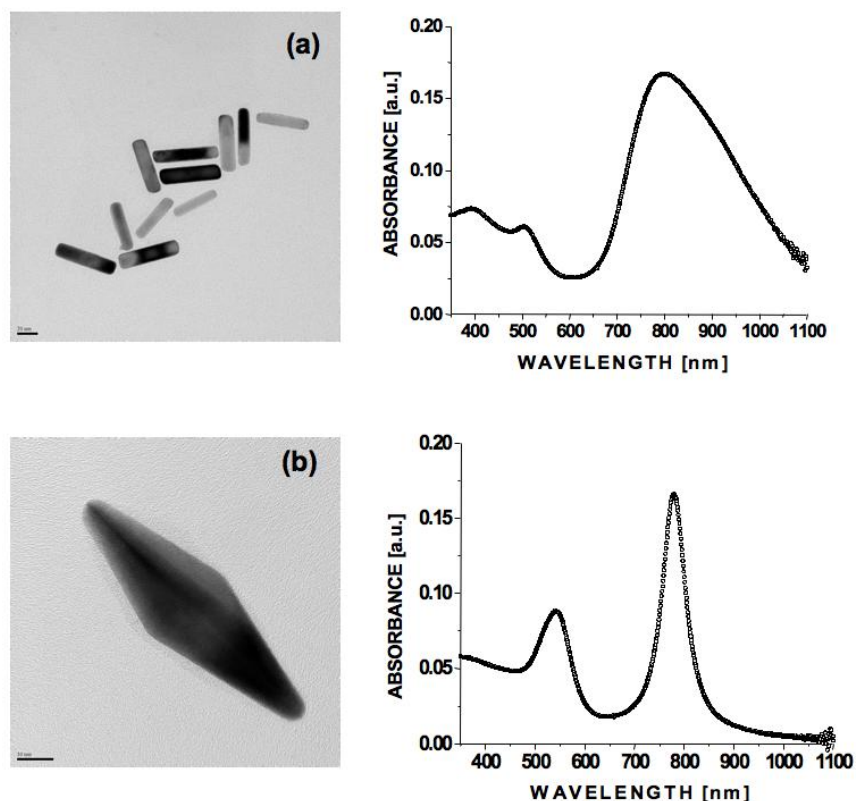


Fig. 3. Transmission-electron microscope images and associated absorption spectra for (a) Au/Ag core/shell nanorods and (b) Au bipyramids in water. The scale bars are (a) 20 nm and (b) 10 nm.

This method produces single-crystal rods with smooth surfaces, controllable aspect ratios, and $> 95\%$ yield. Figure 2(a) shows a transmission-electron-microscope (TEM) image of typical Au nanorods used in the trapping experiments, with an average length of 60 nm and diameter of 13 nm. The aspect ratio of the rods is such that their longitudinal plasmon resonance is centered around 800 nm, as can be seen in the absorption spectrum of Figure 2(b). The relatively broad inhomogeneous linewidth of the spectrum is due to the distribution of rod shapes.

In order to coat Au nanorods with Ag, 0.8 mL of nanorod solution is first diluted in 4 mL of a 1 wt % aqueous solution of polyvinylpyrrolidone (PVP), which acts as a stabilizing agent. Into this solution, 1.0 mM AgNO_3 solution is added, followed by the addition of 0.1 M ascorbic acid and gentle mixing. Reduction of Ag(I) is started by injecting 0.2 mL of 0.1 mM NaOH solution, followed by quick mixing. The reaction completes in less than 5 minutes, and is evidenced by a clear change in the color of the solution. Figure 3(a) shows a TEM image of typical core-shell nanorods used in the trapping experiments, with an average shell thickness of 2 nm. The broadened absorption spectrum reflects the increased inhomogeneity of the core/shell sample, as well as an increased homogeneous linewidth of the plasmon resonance in these particles due to increased interface damping.

In order to produce Au bipyramids, it is necessary to start with multiply twinned seeds, rather the single-crystal particles used to produce nanorods. To produce these seeds, 0.3 mL of freshly prepared 10 mM NaBH₄ is added, at room temperature and under vigorous stirring, to a 20 mL solution containing 0.125 mM HAuCl₄ and 0.25 mM sodium citrate. The gold sol is then aged for at least two hours. Growth of the bipyramids from the seeds then proceeds as for the nanorods. Figure 3(b) shows a typical bipyramid; these particles have an average length of 100 nm and diameter at their widest point of 30 nm. The bipyramids show a remarkable uniformity in their shape, which is reflected in the narrow absorption peak in the ensemble.

3.2 Optical-trapping apparatus

All measurements are performed with a home-built microscopy apparatus, illustrated schematically in Figure 4. The trapping beam is obtained from a tunable, continuous-wave, linearly-polarized Ti:Sapphire laser (Coherent). The beam is spatially filtered to give a high-quality Gaussian mode, and is then sent through a telescope and a tube lens and into a microscope (Nikon). The focal lengths of the lenses in the telescope are chosen such that the beam diameter at the back focal plane of the microscope's water-immersion objective (Olympus APLSAPO 60X) is approximately 10 mm, slightly overfilling the back aperture of the objective and ensuring that the laser is focused to a nearly diffraction-limited spot. Waveplates in the beam path allow arbitrary adjustment of the polarization state of the trapping laser.

The presence of rods in the laser focus can be monitored by imaging back-scattered light onto a CCD camera. However, light scattered by a trapped rod is accompanied by a significant background of light reflected off objective lenses, coverslip surfaces, and other optical elements, so that quantitative measurements are difficult. By contrast, a nearly background-free signal is obtained when the trapped rods are excited by a second, probe beam, derived from a pulsed, tunable Ti:Sapphire laser (Spectra-Physics) and traveling along a parallel path. The probe pulses induce broad-band two-photon fluorescence from trapped rods,²¹ as shown in Figure 1(b).

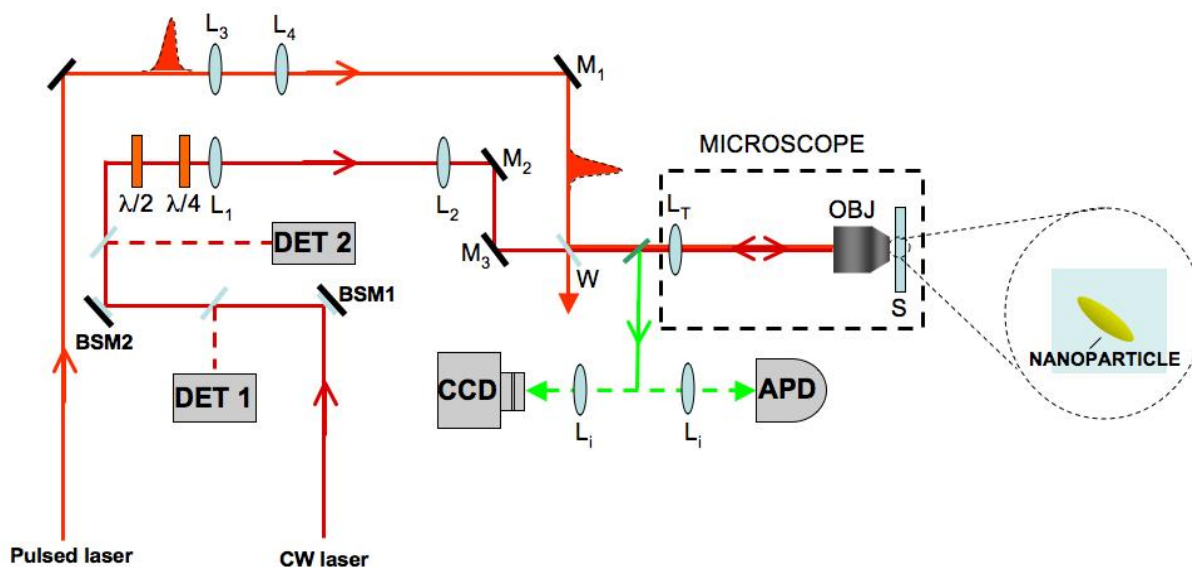


Fig. 4. Experimental trapping setup. Two lasers are used, one for trapping and one for probing of the sample. The beam path used for trapping consists of lenses, L_1 and L_2 , of focal lengths 20 cm and 25 cm, respectively, and steering mirrors M_2 and M_3 . Beam-pointing stability is maintained through the use of beam stabilizing mirrors, BSM_1 and BSM_2 , and position-sensitive detectors, DET_1 and DET_2 . The probe beam path has lenses L_3 and L_4 , of equal focal length 5 cm, and steering mirror M_1 . The beams are spatially combined at window W before entering the microscope. L_T is a tube lens of length 20 cm, and OBJ and S represent the water-immersion objective lens and sample, respectively. Two-photon fluorescence is imaged, using L_i , either onto a CCD camera or APD single-photon detector. The polarization of the probe beam is linear, and the half- and quarter-wave plates are used to generate arbitrary polarization states for the trap beam.

For the experiments reported here, the probe pulses are linearly polarized and spectrally centered around 800 nm, with a pulse duration of less than 100 fs and a repetition rate of 80 MHz. Dispersion encountered by the pulses before the sample is compensated by double passing through a pair of prisms. The probe pulses pass through a 1:1 telescope before being combined with the trap beam *via* a first-surface reflection from a glass window. This configuration allows independent focus and polarization control of the trap and probe beams, which is essential for optimizing the two-photon fluorescence signal from the trapped nanoparticles. The average probe-laser power is maintained at least a factor of ten smaller than that of the trapping laser, in order to minimize its effects on the trapped particles. The emitted fluorescence is collected through the microscope objective, spectrally filtered using a hot mirror and a pair of color filters, and imaged onto either a thermoelectrically-cooled CCD camera (Andor IXON) or a photon-counting avalanche photodiode module (Perkin-Elmer SPCM).

4. RESULTS

4.1 Single-particle trapping trajectories

By monitoring the two-photon fluorescence signal as a function of time, we are able to monitor the particle number in the trap. Figure 5 shows a sample record of the fluorescence signal as a function of time, which we refer to as a “trapping trajectory.” Discrete upwards and downwards steps correspond to individual rods entering and leaving the trap. This trajectory shows a single rod being trapped for approximately 450 seconds. Using a trap-laser wavelength of 850 nm, we have observed trapping times for Au nanorods and bipyramids of up to 20 minutes. Due to the broader linewidth of the Au/Ag core/shell nanorods, stable trapping requires tuning to a wavelength of 880 nm, and maximum trapping times are somewhat reduced.

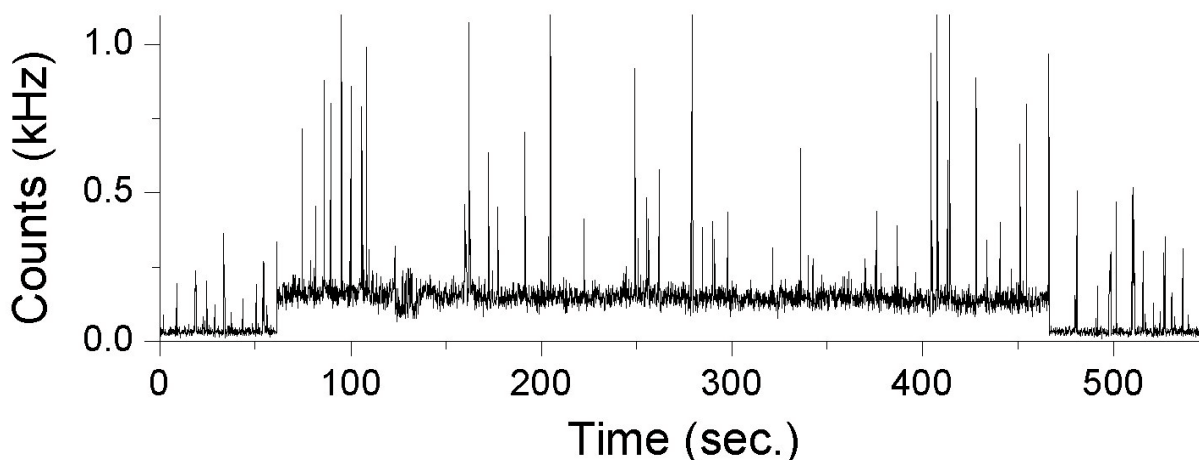


Fig. 5. Time trace of two-photon fluorescence from rods in an optical trap, for a trapping-laser wavelength of 850 nm and power of 140 mW. Two-photon fluorescence was detected with a single-photon counting avalanche photodiode module, and photon counts were grouped into 125-ms time bins.

4.2 Autocorrelation functions

Quantitative information about the trapping dynamics is obtained by measuring the temporal autocorrelation function, $G^{(2)}(\tau)$, of the emitted fluorescence photons, by sending pulses from the single-photon detector to a digital correlator (ALV-6000). Fig. 6(a) shows the measured autocorrelation when the trapping laser is turned off, with the concentration of Au nanorods adjusted such that no more than one rod is in the probe laser focus at a time. There is a distinct 5- μ s

decay, due to rotational diffusion of the rods about their short axes, and a 20-ms decay, due to translational diffusion of the rods through the probe laser spot. The figure also shows a fit to a simple diffusional model.²²

$$G^{(2)}(\tau) = C_1 \exp(-6\theta\tau) + C_2 \left(1 + \frac{4D\tau}{a^2}\right)^{-3/2}, \quad (3)$$

where θ is the rotational diffusion coefficient, D is the translational diffusion coefficient, a is the radius of the laser spot, and C_1 and C_2 are proportionality constants. The best fit is narrower than the experimental curve, due to the distribution of rod sizes in the sample. Nonetheless, the laser spot diameter and average rod length can be determined from the fit by assuming stick boundary conditions for rod diffusion.²³ This yields a spot size of 450 nm, close to the diffraction limit, and an average rod length of 35 nm, in reasonable agreement with the value of 48 ± 9 nm obtained from TEM images. The discrepancy is likely due to the simple model used to describe nanorod diffusion, and to the fact that the longest rods in the ensemble are out of resonance with the probe laser and thus do not contribute to the measured correlation curve.

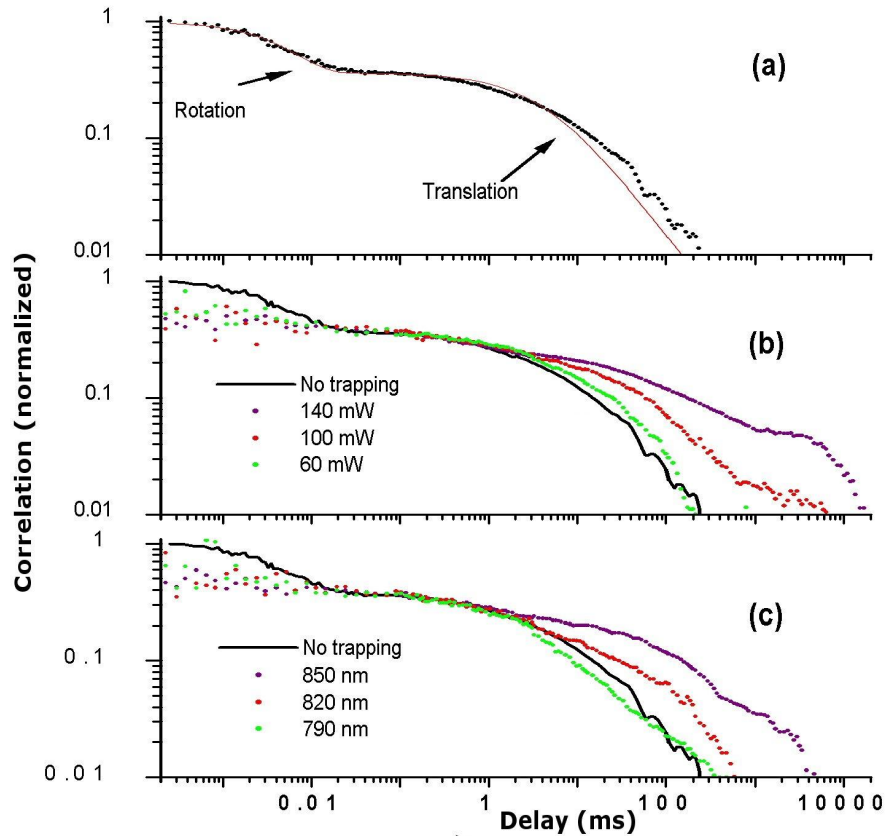


Fig. 6. Intensity autocorrelation functions of two-photon fluorescence from Au nanorods. Each curve is averaged over two 600-sec. integration times. The curves are normalized for ease of comparison. (a) Freely-diffusing rods. Points: measured values; line: theoretical fit. (b) Results for a fixed trapping-laser wavelength of 850 nm. (c) Results for a fixed trapping-laser power of 120 mW.

Figure 6(b) shows the measured autocorrelation functions in the presence of the trapping laser, for different laser powers, I_{trap} . For these measurements, the nanoparticle solution is diluted to the point where rods enter the trap on average once every 10 sec.; this results in a lower signal-to-noise ratio than in the case of freely diffusing rods. There is a clear slowing of translational diffusion, reflecting rods that enter the trapping-laser focus but escape before reaching the center of the trap. The long tail of the correlation function reflects the small fraction of rods that are drawn to the center of the focus and are stably trapped. Figure 6(c) shows the effect of varying the trapping-laser wavelength, λ_{trap} . The residence

time increases relative to free diffusion as λ_{trap} is increased past the 800-nm plasmon resonance. For λ_{trap} shorter than the resonance, rods are repelled from the trap, and the residence time decreases relative to free diffusion.

In addition, the 5- μ s decay is absent in Figs. 6(b) and (c) for all I_{trap} and λ_{trap} . This indicates that the long axes of the rods are oriented relative to the trapping-laser polarization: rotational diffusion around the short axes is suppressed, although the rods are still free to diffuse about their long axis. The light exerts a torque on the rods, proportional to the angle between the laser polarization and the long axis of the rods. As λ_{trap} is tuned through the plasmon resonance, the direction of the exerted torque changes, but the orienting effect remains.

4.3 Single-particle trapping trajectories

The autocorrelation curves provide information about dynamics at short time scales, but are less informative about longer times. Complementary information is therefore obtained by constructing distributions of trapping times from time traces such as the one in Figure 5.

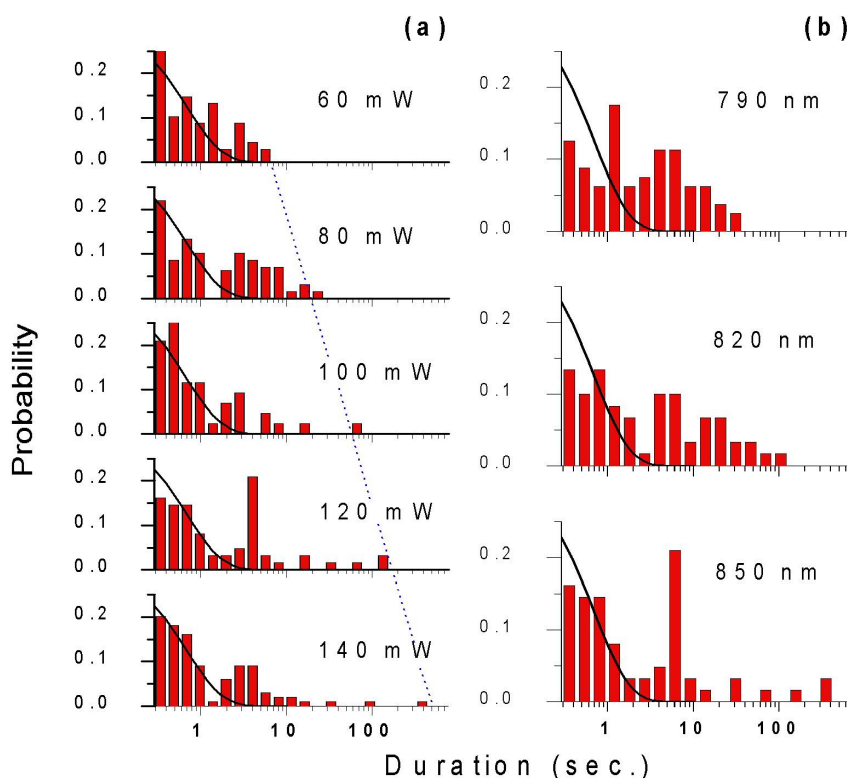


Fig. 7. Histograms of residence times of Au nanorods in the laser focus, binned logarithmically. Each curve is averaged over two 600-sec. integration times. The solid lines show the expected distribution if there were no optical trapping. (a) Results for a fixed trapping-laser wavelength of 850 nm. (b) Results for a fixed trapping-laser power of 120 mW.

The collected time traces have significant shot noise, due to the low fluorescence quantum yield of the rods and the low probe-laser power used. In order to reduce the noise, the photon-count signal is grouped into 125-ms time bins and is processed with a nonlinear, forward- and backward-looking predictive filter.²⁴ This filter efficiently removes noise from underlying signals that undergo abrupt jumps between discrete levels. The filter is applied four times, and a threshold level is then chosen such that only count rates above the threshold are taken to correspond to the presence of a rod in the trap. From the thresholded data, we calculate histograms of the amount of time individual rods spend in the trap, as shown in Figure 7.

The figure also shows the expected distribution of residence times in the absence of any optical forces:²⁵

$$p(t_{\text{trap}}) \approx \exp\left(\frac{-\pi^2 D t_{\text{trap}}}{a^2}\right). \quad (4)$$

The significant difference between this distribution and the measured distributions is a clear sign of optical forces that slow down diffusion of rods through the laser focus. The many short trapping events reflect rods that briefly enter the trapping-laser focus, while the few long events reflect stably trapped rods. The statistics of the histograms and the maximum observable trapping time are limited by the finite observation time: in order to allow several trapping conditions to be compared, the measurement time was limited to 600 sec. Nonetheless, the measured histograms clearly show the influence of optical trapping.

The residence time of the fully trapped particles is expected to follow Kramers' escape rate:

$$t_{\text{trap}} \propto \exp\left(\frac{U}{k_B T}\right), \quad (5)$$

where the trap potential depth, U , (*i.e.*, the effective potential whose gradient is equal to the mean trapping force) is proportional to I_{trap} . This is consistent with the durations of the longest measured trapping events, as indicated by the dotted line in Fig. 7(a). From these results, we can extract an approximate potential depth for $\lambda_{\text{trap}} = 850$ nm of $U / I_{\text{trap}} \approx 0.043 k_B T / \text{mW}$.

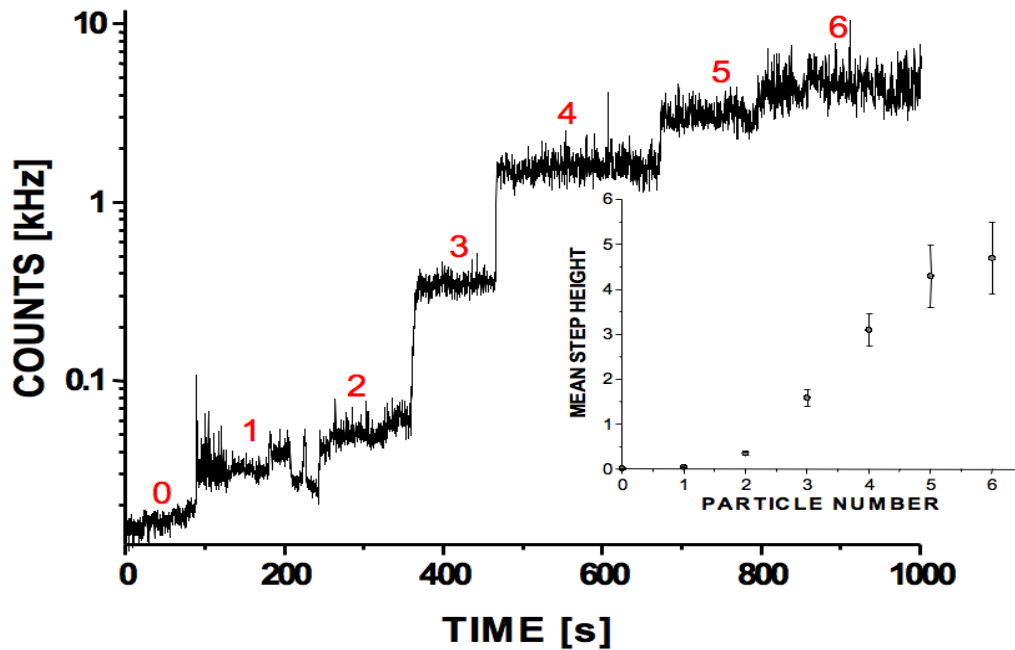


Fig. 8. Time trace showing sequential loading of Au bipyramids into the trap, for a trapping-laser wavelength of 850 nm and power of 140 mW. Counts are obtained by integrating over 66 X 60 pixels of the CCD, with a 100-ms integration time. The numbers 0 – 6 label the stepwise signal changes that occur as particles are progressively loaded into the trap. The inset is a plot of the mean step height as a function of particle number. The error bars represent the standard deviation for each step.

4.4 Multiple-particle trapping

Since the nanoparticles are small compared to the volume of the diffraction-limited laser spot, it is possible to load multiple particles into the trap simultaneously. Figure 8 shows a trapping trajectory with several upwards steps, each one corresponding to the loading of a single Au bipyramid into the trap. Similar trajectories have shown stable trapping of multiple particles for several minutes.

Although the power density of the trapping laser is rather high, we do not see evidence of particle damage or aggregation. Particle damage would result in a large blue shift of the plasmon resonance,¹⁴ and is therefore incompatible with stable trapping. As well, heating sufficient to cause particle melting would also lead to boiling of the surrounding water, which is not observed. Aggregation of the particles would also lead to large resonance shifts and ejection from the trap; moreover, we commonly observe single downwards steps in trapping trajectories, indicating that one particle has escaped while the others remain in the trap.

4.5 Interparticle interactions

Examination of Figure 8, as well as other trapping trajectories such as the one shown in Figure 5, indicates that the two-photon fluorescence signal is not simply proportional to the number of particles in the trap. The inset of Figure 8 illustrates this more clearly, by plotting the mean fluorescence signal as a function of particle number. Since independence of the particles would result in a linear dependence of fluorescence on particle number, the nonlinear dependence suggests the existence of interactions among the trapped particles.

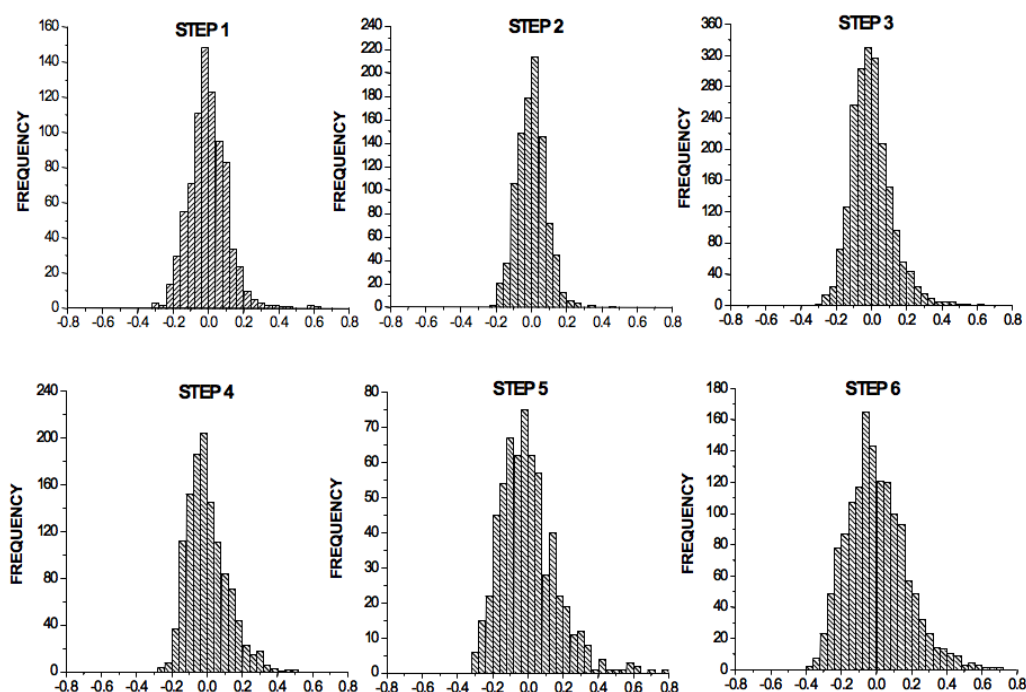


Fig. 9. Histograms of instantaneous two-photon fluorescence intensity, corresponding to each of the steps in Figure 8. Each distribution is normalized by the mean value for the associated step.

Additional evidence for interparticle interactions can be obtained by examining the fluctuations in the fluorescence signal as a function of particle number. For independent particles, one would expect Poissonian statistics, meaning that

the variance in the signal would be proportional to the mean value; as shown in Figure 9 and summarized in Table 1, the variance increases faster than the mean. As well, the distributions exhibit a positive skew, particularly for larger particle number. These results are consistent with interactions among the trapped particles: fluctuations in the particle configuration will lead, through the optical interactions, to fluctuations in the fluorescence signal, with larger effects for a greater number of interacting particles. Moreover, the weakest signal will occur in the absence of interactions, so that fluctuations that increase interactions will increase the fluorescence signal, leading to the skew in the distribution towards greater values.

Excitation of plasmon resonances leads to the strong enhancement of local fields around the particles; finite-difference time-domain calculations indicate that these enhanced fields extend approximately 50 nm from the ends of the bipyramids.²⁶ The localized fields from adjacent particles in the trap may therefore overlap, producing interactions between the induced polarizations in the particles. The stable trapping of multiple particles, though, implies constraints on the possible optical interactions. A strong interaction between particles arranged end-to-end would lead to a red shift in the plasmon resonance, and would thus cause the particles to leave the trap. Conversely, a side-by-side arrangement of the particles could result in a blue shift of the resonance, which is compatible with stable trapping as long as the magnitude of the blue shift is relatively small (less than 10 nm).

Table 1. Variance of two-photon fluorescence for each of the steps in Figure 8, normalized by the mean value for the corresponding step. The variance for step “0”, corresponding to detection noise, is included for reference.

Step	Variance / Mean
0	0.023
1	0.009
2	0.006
3	0.009
4	0.010
5	0.020
6	0.026

Alternatively, the trapping laser may induce effective mechanical interactions among the trapped particles.²⁷ The dipole moment induced in one particle can interact with the moment induced by another particle, leading to forces between the particles; the magnitude and direction of these forces depends on the separation and relative orientation of the particles, as well as their position in the trap and their orientation relative to the laser polarization. When multiple nanoparticles are held in the trap, these optically-induced forces can prevent their aggregation and lead to their arrangement in particular stable configurations, analogous to the optical binding of micrometer-scale dielectric particles.²⁸ Evidence for spatial ordering of the trapped particles comes from the profile of two-photon fluorescence from trapped bipyramids, as shown in Figure 10. The diameter of the two-photon fluorescence spot increases with particle number, and a dip appears in the center of the profile for five trapped particles, consistent with changes in the configuration of the particles as the number of trapped particles increases. This result thus points towards optically induced self-assembly of trapped nanoparticles, which may serve as a convenient method for arranging nanoscale materials into controlled configurations.

5. CONCLUSIONS

We have demonstrated for the first time that material resonances can be used to enhance optical forces on particles in solution, making it possible to orient and position individual metal nanorods and bipyramids in three dimensions. Sequential loading of the trap allows the study of electromagnetic interactions among particles. Nanoparticle assemblies can form spontaneously in the traps as the result of optically-induced interparticle forces. Further measurements on

multiple trapped particles will elucidate the nature and magnitude of these forces and may lead to the controlled fabrication of nanoparticle assemblies.

In addition, the selectivity of the optical forces to the plasmon resonance frequency means that optical traps could be used to sort metal nanoparticles. By flowing nanoparticle solutions through arrays of optical traps, highly selective separation should be possible;²⁹ unlike most other fractionation techniques, this method would be sensitive to the particle shape. Finally, a trapped nanoparticle could serve as a local probe for plasmon-assisted microscopy.³⁰ It should be possible, for example, to scan the particle through a sample and monitor changes in its linear scattering spectrum, measuring local dielectric functions; changes in locally-enhanced Raman scattering, measuring local chemical composition; or changes in diffusion coefficients, measuring local viscosity. Studies to determine the feasibility of this scheme will include the measurement of nanoparticle heating in the trap and its dependence on trapping-laser intensity and wavelength.

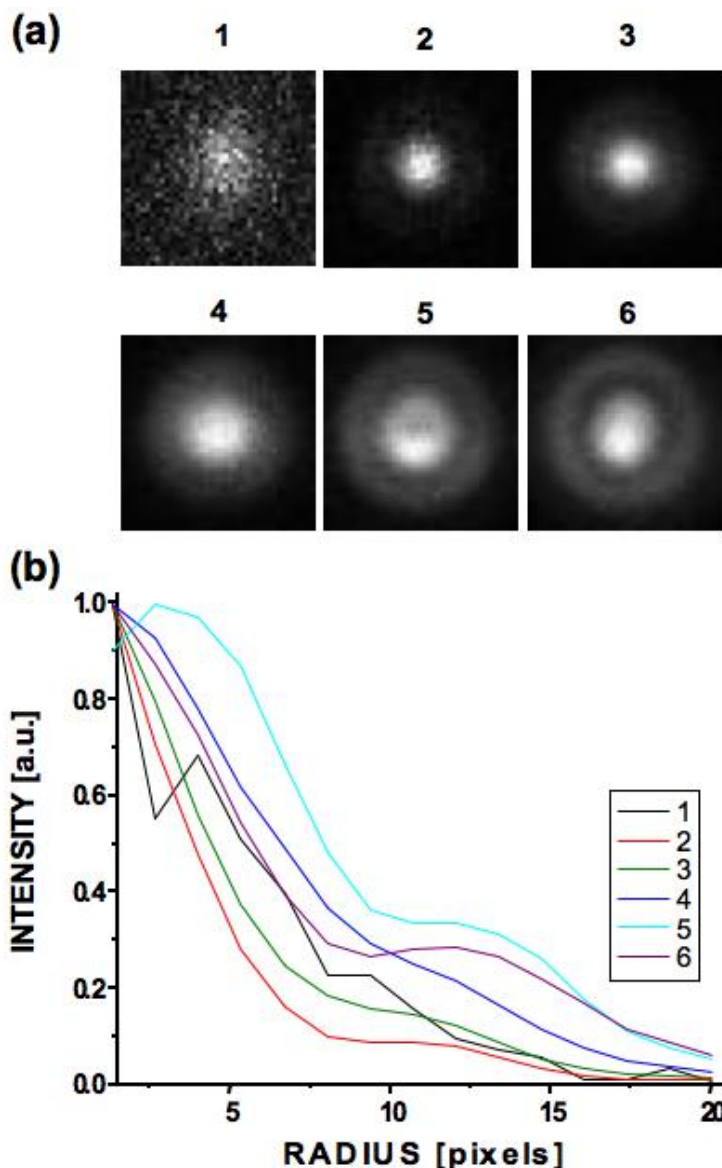


Fig. 10. (a) Sequential images of two-photon fluorescence from trapped bipyramids, as recorded by the CCD camera. Each panel is integrated over 100 ms and is rescaled in intensity. The panel numbers correspond to the steps in Figure 8. (b) Radial profiles for each of the images, normalized to peak intensity. Note that curve “1” has a background contribution that is not insignificant compared to the signal from the particle.

ACKNOWLEDGEMENTS

We thank Dr. J. E. Jureller for experimental assistance, Prof. D. G. Grier for valuable advice, and Prof. A. Dinner for insightful conversations. This work was partially supported by the NSF (grants CHE-0321232 and CHE-0616663). M.L. is supported by the University of Chicago MRSEC NSF-DMR (grant DMR-0213745). K.C.T. acknowledges support from the NSF (DBI-0511849). M.P. and N.F.S. acknowledge support from the Center for Nanoscale Materials, which is supported by the U. S. Department of Energy, Office of Science, Office of Basic Energy Sciences, under contract No. DE-AC02-06CH11357. N.F.S. acknowledges the John S. Guggenheim Foundation for a fellowship.

REFERENCES

1. D. G. Grier, "A revolution in optical manipulation," *Nature* **424**, 810-816 (2003); A. Ashkin, *Optical Trapping and Manipulation of Neutral Particles Using Lasers* (World Scientific, 2006); K. Dholakia and P. Reece, "Optical micromanipulation takes hold," *Nano Today* **1**, 18-27 (2006).
2. J. Plewa, E. Tanner, D. M. Mueth, and D. G. Grier, "Processing carbon nanotubes with holographic optical tweezers," *Opt. Express* **12**, 1978-1981 (2004); S. Tan, H. A. Lopez, C. W. Cai, and Y. Zhang, "Optical trapping of single-walled carbon nanotubes," *Nano Lett.* **4**, 1415-1419 (2004).
3. R. Agarwal, K. Ladavac, Y. Roichman, G. Yu, C. M. Lieber, and D. G. Grier, "Manipulation and assembly of nanowires with holographic optical traps," *Opt. Express* **13**, 8906-8912 (2005).
4. K. Svoboda and S. M. Block, "Optical trapping of metallic Rayleigh particles," *Opt. Lett.* **19**, 930-932 (1994); P. M. Hansen, V. K. Bhatia, N. Harrit, and L. Oddershede, "Expanding the optical trapping range of gold nanoparticles," *Nano Lett.* **5**, 1937-1942 (2005).
5. J. Prikulis, F. Svedberg, M. Käll, J. Enger, K. Ramser, M. Goksör, and D. Hanstorp, "Optical spectroscopy of single trapped metal nanoparticles in solution," *Nano Lett.* **4**, 115-118 (2004).
6. Y. Seol, A. E. Carpenter, and T. T. Perkins, "Gold nanoparticles: Enhanced optical trapping and sensitivity coupled with significant heating," *Opt. Lett.* **31**, 2429-2431 (2006).
7. A. Ashkin and J. M. Dziedzic, "Observation of resonances in the radiation pressure on dielectric spheres," *Phys. Rev. Lett.* **38**, 1351-1354 (1977).
8. A. Ashkin, J. M. Dziedzic, J. E. Bjorkholm, and S. Chu, "Observation of a single-beam gradient force optical trap for dielectric particles," *Opt. Lett.* **11**, 288-290 (1986).
9. S. Chu, J. E. Bjorkholm, A. Ashkin, and A. Cable, "Experimental observation of optically trapped atoms," *Phys. Rev. Lett.* **57**, 314-317 (1986).
10. R. R. Agayan, F. Gittes, R. Kopelman, and C. F. Schmidt, "Optical trapping near resonance absorption," *Appl. Opt.* **41**, 2318-2327 (2002).
11. D. T. Chiu and R. N. Zare, "Biased diffusion, optical trapping, and manipulation of single molecules in solution," *J. Am. Chem. Soc.* **118**, 6512-6513 (1996); M. A. Osborne, S. Balabramanian, W. S. Furey, and D. Klennerman, "Optically biased diffusion of single molecules studied by confocal fluorescence microscopy," *J. Phys. Chem. B* **102**, 3160-3167 (1998).
12. T. Iida and H. Ishihara, "Theoretical study of the optical manipulation of semiconductor nanoparticles under an excitonic resonance condition," *Phys. Rev. Lett.* **90**, 057403 (2003).
13. M. Pelton, "Comment on 'Theoretical study of the optical manipulation of semiconductor nanoparticles under an excitonic resonance condition'," *Phys. Rev. Lett.* **92**, 89701 (2004).
14. M. Pelton, M. Liu, S. Park, N. F. Scherer, and P. Guyot-Sionnest, "Ultrafast resonant optical scattering from single gold nanorods: Large nonlinearities and plasmon saturation," *Phys. Rev. B* **73**, 155419 (2006).
15. C. F. Bohren and D. R. Huffman, *Absorption and Scattering of Light by Small Particles* (John Wiley & Sons, New York, 1983).
16. M. Pelton, M. Liu, H. Y. Kim, G. Smith, P. Guyot-Sionnest, and N. F. Scherer, "Optical trapping and alignment of single gold nanorods by using plasmon resonances," *Opt. Lett.* **31**, 2075-2077 (2006).

17. K. C. Toussaint, Jr., M. Liu, M. Pelton, J. Pesic, M. J. Guffey, P. Guyot-Sionnest, and N. F. Scherer, University of Chicago and Argonne National Laboratory, unpublished information (2007).
18. J. R. Arias-González and M. Nieto-Vesperinas, "Optical forces on small particles: attractive and repulsive nature and plasmon-resonance conditions," *J. Opt. Soc. Am A* **20**, 1201-1209 (2003); A. S. Zelenina, R. Quidant, G. Cadenes, and M. Nieto-Vesperinas, "Tunable optical sorting and manipulation of nanoparticles via plasmon excitation," *Opt. Lett.* **31**, 2054-2056 (2006).
19. P. B. Johnson and R. W. Christy, "Optical constants of the noble metals," *Phys. Rev. B* **88**, 077402 (2002).
20. N. R. Jana, L. Gearhart, and C. J. Murphy, "Seed-mediated growth approach for shape-controlled synthesis of spheroidal and rod-like gold nanoparticles using a surfactant template," *Adv. Mater.* **13**, 1389-1393 (2001); B. Nikoobakht and M. A. El-Sayed, "Preparation and growth mechanism of gold nanorods (NRs) using seed-mediated growth method," *Chem. Mater.* **15**, 1957-1962 (2003); M. Liu and P. Guyot-Sionnest "Synthesis and optical characterization of Au/Ag core/shell nanorods", *J. Phys. Chem. B* **108**, 5882-5888 (2004); M. Liu and P. Guyot-Sionnest, "Mechanism of silver(I)-assisted growth of gold nanorods and bipyramids," *J. Phys. Chem. B* **109**, 22192-22200 (2005).
21. R. A. Farrer, F. L. Butterfield, V. W. Chen, and J. T. Fourkas, "Highly efficient multiphoton-absorption-induced luminescence from gold nanoparticles," *Nano Lett.* **5**, 1139-1142 (2005); H. Wang, T. B. Huff, D. A. Zweifel, W. He, P. S. Low, A. Wei, and J.-X. Cheng, "In vitro and in vivo two-photon luminescence imaging of single gold nanorods," *Proc. Natl. Acad. Sci. USA* **102**, 15752-15756 (2005).
22. R. Rigler and E. S. Elson, Eds., *Fluorescence Correlation Spectroscopy: Theory and Applications* (Springer, Berlin, 2001).
23. R. Vansathi, S. Ravichandran, and B. Bagchi, "Needlelike motion of prolate ellipsoids in the sea of spheres," *J. Chem Phys.*, **114**, 7989-7992 (2001).
24. S. H. Chung and R. A. Kennedy, "Forward-backward non-linear filtering technique for extracting small biological signals from noise," *J. Neurosci. Methods* **40**, 71-86 (1991).
25. G. Zumofen, J. Hohlbein, and C. G. Hübner, "Recurrence and photon statistics in fluorescence fluctuation spectroscopy," *Phys. Rev. Lett.* **93**, 260601 (2004).
26. M. Liu, S. K. Gray, and P. Guyot-Sionnest, manuscript in progress.
27. H. Xu and M. Xäll, "Surface-plasmon-enhanced optical forces in silver nanoaggregates," *Phys. Rev. Lett.* **89**, 246802 (2002); A. J. Hallock, P. L. Redmond, and L. E. Brus, "Optical forces between metallic particles," *Proc. Natl. Acad. Sci. USA* **102**, 1280-1284 (2005); A. Zelenina, R. Quidant, and M. Nieto-Vesperinas, "Enhanced optical forced between coupled resonant metal nanoparticles," *Opt. Lett.* **32**, 1156-1158 (2007).
28. M. M. Burns, J.-M. Fournier, and J. A. Golovchenko, "Optical binding," *Phys. Rev. Lett.* **63**, 1233-1236 (1989).
29. K. Ladavac, K. Kasza, and D. G. Grier, "Sorting mesoscopic objects with periodic potential landscapes: Optical fractionation," *Phys. Rev. E* **70**, 101901 (2004); M. Pelton, K. Ladavac, and D. G. Grier, "Transport and fractionation in periodic potential-energy landscapes," *Phys. Rev. E* **70**, 031108 (2004).
30. J. Wessel, "Surface-enhanced optical microscopy," *J. Opt. Soc. Am. B* **2**, 1538-1541 (1985).